INTERNATIONAL JOURNAL OF NUMERICAL MODELLING: ELECTRONIC NETWORKS, DEVICES AND FIELDS
Int. J. Numer. Model. 2009; **22**:201–218
Published online 18 December 2008 in Wiley InterScience (www.interscience.wiley.com). DOI: 10.1002/jnm.709

Positional dependence of FDTD mode detection in photonic crystal systems

G. A. Stark[1,*,†], M. Mishrikey[2], F. Robin[1], H. Jaeckel[1], C. Hafner[2], R. Vahldieck[2] and D. Erni[3]

[1]*Electronics Laboratory, ETH Zurich, CH-8092 Zurich, Switzerland*
[2]*Laboratory of Electromagnetic Fields and Microwave Electronics, ETH Zurich, CH-8092 Zurich, Switzerland*
[3]*General and Theoretical Electrical Engineering (ATE), University of Duisburg-Essen, D-47048 Duisburg, Germany*

SUMMARY

We have developed an algorithm for evaluating the accuracy and reliability of photonic crystal (PhC) simulations, and used it to analyze the influence of excitation and detector placement in finite-difference time-domain algorithm (FDTD) simulations of two canonical PhC systems. In order to perform this computationally expensive analysis, we evaluated the use of filter diagonalization as an alternative to the Fourier Transform for mode detection, and developed a parallelization algorithm to take advantage of the inherent concurrency in simulating periodic systems. A map of locations where mode detection fails was generated, and we show that this is equivalent to a map of the node densities of the system. In addition to the expected high nodal densities at the symmetry areas of each system, we find more difficult to characterize patterns of high nodal density for the higher-order modes. Based on the observed behavior we are able to provide concrete rules to optimize the detection and excitation of modes in FDTD simulations of PhC systems. Although PhCs were studied, the presented strategies and results apply to the much broader class of all computational time-domain problems where Bloch–Floquet boundary conditions are used. Copyright © 2008 John Wiley & Sons, Ltd.

Received 15 January 2008; Revised 17 July 2008; Accepted 23 September 2008

KEY WORDS: photonic crystals; FDTD; periodic

1. INTRODUCTION AND OVERVIEW

Photonic crystals (PhCs) are periodic structures that provide a powerful tool for controlling the flow of light. In particular, PhC waveguide devices are investigated for use in a wide range of applications, such as lasing [1] and all-optical switches [2].

A common design goal is to customize a PhC device's properties for a particular application. For example, one might seek to maximize the band gap of a PhC lattice geometry, or the slow

*Correspondence to: G. A. Stark, Electronics Laboratory, ETH Zurich, CH-8092 Zurich, Switzerland.
†E-mail: stark@ife.ee.ethz.ch

light properties of certain modes in a PhC waveguide. In these situations, it is desirable to employ an optimization algorithm such as a downhill-simplex or evolutionary algorithm. In these circumstances the robustness, computational cost, and accuracy of the simulation technique become critical. A false mode (the erroneous detection of a non-existent mode), or missed mode (an existing mode that fails to be detected) will cause optimization algorithms to fail, and the simulation will be called many times in the course of finding the optimal solution.

We research the use of the finite-difference time-domain algorithm (FDTD) for PhC design. While alternatives such as plane-wave expansion [3] and the multiple multipole method [4] exist, FDTD supports broadband simulations, metallic and absorbing boundary conditions, arbitrary geometries, dispersive, non-linear, and inhomogeneous materials with complicated structures. FDTD also scales differently than other methods, making it the most computationally efficient method for some problems (see the discussion in [5]). While the FDTD approach is very flexible, experience is required to obtain robust and accurate results necessary for the automatic evaluation of band gap behavior. This paper studies a phenomenon in FDTD PhC simulations, which is often glossed over, or left to trial and error: the effect of sensor/excitation position on mode detection. We find that there is a significant impact, determined by the symmetries of the system, and that our map of points where the detection fails is a map of the nodal density of the system being investigated.

To analyze the effects of the sensor/excitation position, we study two canonical PhC problems, the calculation of band diagrams (BDs) for PhCs based on (1) a square lattice and (2) a triangular lattice of dieletric rods in air. Were one solely interested in the BDs of these systems, one would (under normal circumstances) be better off using a plane-wave method. We choose these systems because they are well understood, characteristic of the problems involved in simulating PhC systems using FDTD, and because independant algorithms exist to evaluate the results. This allows us to isolate the effects of the positional dependance. We developed a simple algorithm for evaluating the results of a PhC simulation, which generates statistics quantifying the robustness and accuracy of the mode finding. In order to isolate the positional-dependence errors it was necessary to impose rigorous constraints on the other sources of numerical error, namely the measurement time and grid size. To accomplish this we again employed our evaluation algorithm, the results of which are also useful.

In Section 2 we discuss the computational methods used. We first present the algorithm for FDTD analysis of PhC devices, and identify the areas where errors, false, or missed modes can occur. This is followed by our algorithm for evaluating the accuracy and reliability of PhC simulations, and a description of a parallelization strategy that results in perfectly linear speedup.

The rest of the methodology section shows how we were able to obtain the accuracy we required without exploding computational costs: the use of effective permittivities and filter diagonalization for mode detection. Without algorithmic changes, FDTD can give arbitrary accuracy with an increase in computational expense, but computational cost is a limiting factor in many investigations, including our own. For this reason it is worthwhile to evaluate more recent FDTD techniques. In Section 2 we apply our evaluation algorithm to evaluate the benefits of the above mentioned, while showing how we are able to guarantee the accuracy of our simulations.

In Section 3 we use the evaluation algorithm to analyze the spatial dependence of the excitation and detection of modes in two canonical problems, the BD calculation of PhCs based

DOI: 10.1002/jnm

on (1) a square lattice and (2) a triangular lattice of dielectric rods in air. We present maps showing the spatial sensitivity of mode detection, and show that these are equivalently maps of density of nodes in a PhC. For the lower-order modes, we find that the node densities are easily predicted, being trivially dependent on the symmetries of the system. We find, however, that for the higher-order modes more interesting behavior occurs. This gives us some general insight into the choice of detector positioning, and some preliminary insight regarding systems with high densities of modes.

Although the results presented in Section 3 are generated for PhC systems, they apply to any periodic system where Bloch–Floquet boundary conditions are used. The results of Section 2.4.2 should be of interest to anyone still using the Fourier transform for mode detection, and Section 2.4.1 for those not yet using effective-permitivities.

2. METHODOLOGY

2.1. Mode detection algorithm

The FDTD 'Order-N' method for mode detection in periodic structures was first proposed as an alternative to the plane-wave expansion method with improved scalability with respect to the number of grid cells. The algorithm can be outlined as:

Algorithm 1 FDTD band-diagram generation.

Create the computational domain in FDTD: a single unit cell of the crystal being investigated.
for each **k** in the irreducible Brillouin zone (IBZ) **do**
  Apply Bloch boundry conditions $\mathbf{F}(\mathbf{r}+\mathbf{L}) = e^{j\mathbf{k}\cdot\mathbf{L}}\mathbf{F}(\mathbf{r})$, where **F** is a complex field quantity, **E** or **H**.
  Excite the computational domain.
  Measure a field component for some time T
  Determin modal frequencies from the time-domain data.
end for

This concise outline masks subtleties in implementation that can greatly impact the performance of the algorithm with respect to accuracy, reliability, and computational cost. Results can be negatively affected by insufficient grid resolution, insufficient measurement time T, failing to excite a mode of interest, and failing to detect a mode of interest. Detection failure can occur as a result of an insufficient measurement time, and both detection and excitation can fail due to measuring or exciting the field near the location of a node of mode(s) of interest.

The sources of error due to grid resolution and measurement time are well-studied problems. Some techniques for mitigating them can be found in the literature, for example [6], and the problem remains an active area of research. We have applied and studied two such techniques in the course of our investigation. They are discussed in Sections 2.4.1 and 2.4.2, respectively.

The choice of field measurement location is, however, seldom discussed, and typically left to the judgment of the user. Choosing a single measurement location can lead to missed modes,

DOI: 10.1002/jnm

while performing spectral analysis on a many measurement points becomes computationally expensive. The occasional missed mode is not critical when generating BDs for well-understood systems, but when the mode detection algorithm is to be integrated into an optimization routine, or when the system being analyzed is complex and difficult to understand, such errors become important.

In this investigation, the common method of placing a dipole at the measurement location, and exciting a Gaussian pulse was used to excite the fields. Because the failure mechanism behind the positional dependence of detector location is the same as that behind the positional dependence of the source location, i.e. the sensor or the dipole is placed at a modal node point, discussing one is equivalent to discussing the other. The technique used for mode detection is discussed in detail in Section 2.4.2.

2.1.1. Triangular lattice simulation. It is not entirely trivial to extend the algorithm described above to other PhC lattice types. Here we consider the example of a triangular lattice. Because the standard FDTD algorithm applies only to rectangular grids, it is necessary to simulate over a unit cell that is greater than the primitive unit cell (this can be seen in the sensormaps, e.g. Figure 11). This results in simulating a 'folded' version of the real band structure. There are two solutions to this problem, both of which can be read about in detail in Chapter 16.11 of [6].

The first solution, employed here, is to replicate the dipole source in the same spot of each copy of the primitive cell represented within the larger grid being simulated, adjusted by the correct Bloch phase factor. Then one places a duplicate sensor in the folded region, and compares the modes found by both sensors, ensuring that they differ only by a small amount in the phase factor (here chosen to be $\leqslant 0.1$) and frequency (here chosen to be $\leqslant 1e{-}3$).

A second solution, which we believe to be the superior (for reasons we discuss below in Section 3), is to take the smallest rectangle in which one can inscribe the correct rhomboidal primitive unit cell, perform the standard FDTD algorithm over the entire grid, and then apply modified boundary conditions over rhombus describing the primitive unit cell (again, see [6] Chapter 16.11 for details).

In practice, one finds the former approach to be very common, because it can be done entirely in post-processing, and does not require modification of the underlying FDTD code. For this reason, we have chosen this approach for our study of the positional dependence. As we shall see in Section 3, however, our results seem to weigh in favor of the latter approach.

2.2. Benchmarking

In practice it is often difficult to determine what is to blame when faced with errors or missed modes. To address this problem we have developed an algorithm for evaluating the quality of mode detection results. The algorithm is based on comparing a test BD against a reference BD. We define:

$\mathscr{D}$ a maximum distance in frequency, for which two modes are considered to match. This is chosen to be much greater than the expected errors (in these investigations $\mathscr{D}=0.02$, in reduced frequency, see Section 2.3). Introducing this cut-off distance is necessary to gather statistics on the percentage of found modes (reliability) and the error (accuracy), in order to prevent mismatching modes.

DOI: 10.1002/jnm

$\mathrm{TST}_{\mathbf{k}} = t_1 \ldots t_N$ The set of modes to be tested.
$\mathrm{REF}_{\mathbf{k}} = r_1 \ldots r_M$ The set of reference modes.
$u_{\min}$ **and** $u_{\max}$ The minimum and maximum frequencies over which to compile results.
missed modes The count of modes for which no match was found.
matched modes The count of modes for which matches were found.
$\mathtt{err}_{\mathtt{m}}$ $\mathtt{max}(|u_{\mathtt{ref}} - u_{\mathtt{test}}|)$ for the mth matched mode.
The algorithm is then:

Algorithm 2 Algorithm for calculating errors and missed modes for a particular **k**.

```
m = 0.
for r_i ∈ REF_k do
  if u_min ≤ r_i ≤ u_max then
    Find the nearest test mode t_j.
    if |r_i − t_j| > 𝒟 then
      ++Missed mode count.
      Remove r_i from REF_k.
    else
      ++m
      Compute err_m
      Remove r_i from REF_k.
      remove t_j from TST_k
    end if
  end if
end for
err_avg = <err_m>.
err_max = max(err_m).
Matched mode count = m.
```

In the investigations in this paper, $\mathrm{REF}_{\mathbf{k}}$ were produced using the plane-wave expansion method [3], configured to provide results accurate to 1×10^{-7}. In the absence of a reliable reference result, the algorithm must be used as a part of a standard convergence analysis.

We applied the algorithm to two canonical problems, the BD of a 2D square lattice of dielectric rods ($\epsilon = 8.9$) in air ($\epsilon = 1.0$), with radius to lattice constant ratio $r/a = 0.2$, and a triangular lattice of rods ($\epsilon = 12.0$), again in air with $r/a = 0.2$. The results in Section 3 were obtained by placing point sources (dipole Gaussian pulses) and detectors, located at 100×100 positions for the square lattice, and 100×150 positions for the triangular lattice, evenly spaced across a single FDTD cell. For each point on the grid, an FDTD simulation was performed, and the benchmarking algorithm performed on the resulting modal data. Note then that all results in this paper represent the results of applying algorithm 2.2 to all 40**k** of a complete BD.

Prior to this, however, Algorithm 2 was applied to eliminate all other sources of error. The results of this investigation are discussed below.

2.3. Units

When studying PhCs, it is conventional to work in systems of scale invariant units [7], which we do throughout this paper. Frequencies are expressed in units of $[a/\lambda]$, time in units of $[a/c]$, and k-vectors in units of $[2\pi/a]$, where a is the crystal lattice constant.

DOI: 10.1002/jnm

2.4. Errors

As mentioned, there are several sources of error in FDTD simulations, including discretization error and errors arising from the information uncertainty principle, i.e. an insufficient measurement time. These errors must be understood before relying on simulation results. Prior to performing the positional experiments, the benchmarking algorithm was used to determine proper choice of grid resolution and measurement time, by fixing one parameter to an initial guess, and obtaining the value to which the error converged in the other. This allowed us to rapidly determine the grid resolution and measurement time needed to obtain a desired precision.

Rather than employ a brute-force approach to reducing computational errors, by employing increasing grid resolutions and measurement times, it is worth considering recent advances in sub-pixel smoothing and spectral analysis. The techniques we employed offer compelling benefits, so we discuss them here in order to show how we achieved our rigorous error constraints.

2.4.1. Grid size. A first step in performing simulations using FDTD is to determine the grid size needed for the required accuracy. In the absence of a reference solution this can be done by calculating the extent to which solutions change as a function of grid size. This grid resolution can be greatly reduced by employing sub-pixel smoothing. In our case we use a method which been studied extensively on PhC systems [8]. As we see in Figure 1, this has a dramatic effect on both the magnitude of the error and the smoothness of the convergence. Note the sharp fluctuations in error without averaging caused by stair casing effects. This highlights a key benefits of sub-pixel averaging—by smoothing the convergence curve, it greatly simplifies the

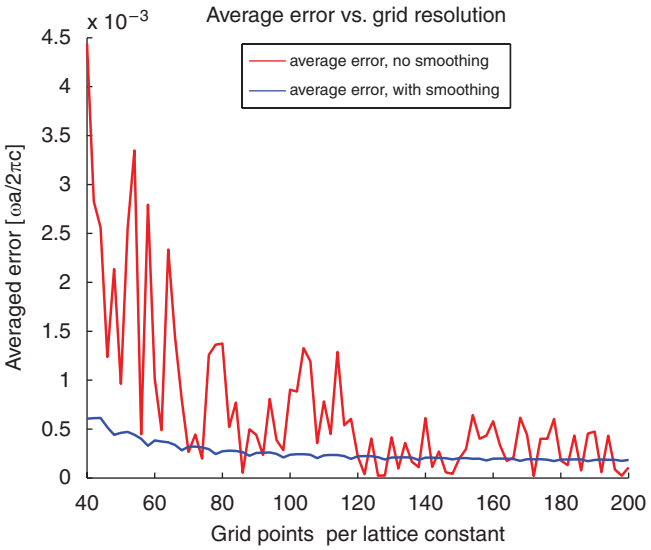

Figure 1. Average error in the square lattice simulations as a function of grid resolution, with and without sub-pixel smoothing.

DOI: 10.1002/jnm

determination of an appropriate grid size. Based on the results in Figure 1 we chose a 50×50 grid (with smoothing), which gives us $\mathtt{err}_{\max} \leqslant 0.02$, and $\mathtt{err}_{\mathrm{avg}} \leqslant 0.5\mathrm{e}-3$.

2.4.2. Measurement duration. Obtaining harmonic information from a set of time data is a fundamental problem in many fields. One approach is to Fourier transform the time signal, and execute a peak detection algorithm on the resulting spectra. This approach fails to take advantage of recent advances in the field [9]. One recent alternative is the filter diagonalization approach, which we have tested here.

The Fourier transform is governed by the information uncertainty principle, which states that the resolution in frequency bin $\Delta\omega$ is inversely proportional to the length $N\Delta t$ of the time signal:

$$\Delta\omega = \frac{2\pi}{N\Delta t} \tag{1}$$

When highly accurate frequency information is needed, the Fourier transform requires a very long time signal. In an FDTD simulation, this corresponds to a long simulation duration.

Significant progress in the numerical technique for harmonic inversion was made by Wall and Neuhauser who developed an algorithm based on filter diagonalization in 1994 [10]. The method weakens the uncertainty principle by formulating the harmonic inversion problem as a non-linear fitting problem, recasting the non-linear problem as a linear algebraic one, and then using a filter-diagonalization scheme to find a solution. In practice this means a greatly reduced sample size is needed for a given accuracy, as we see in Figure 2.

Filter diagonalization has already been suggested for use in FDTD simulation of periodic structures [11], where the method's superiority in discerning closely spaced frequencies was demonstrated. We have expanded on this analysis by comparing the reliability and accuracy

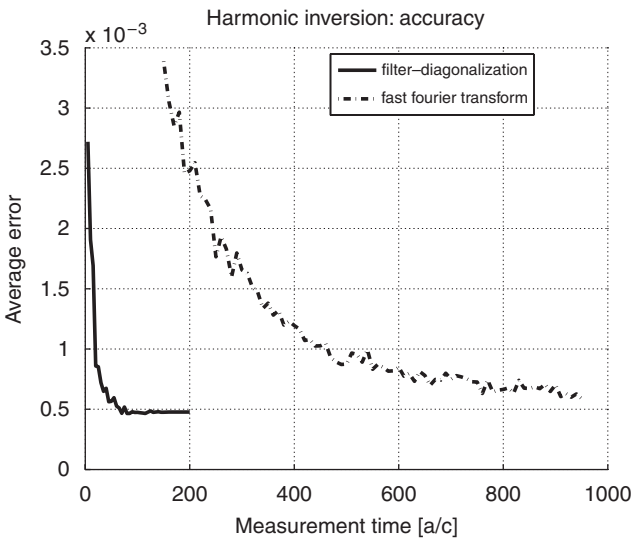

Figure 2. Error analysis of frequency diagonalization against measurement time, compared with the Fourier transform. Results shown for the square lattice case.

DOI: 10.1002/jnm

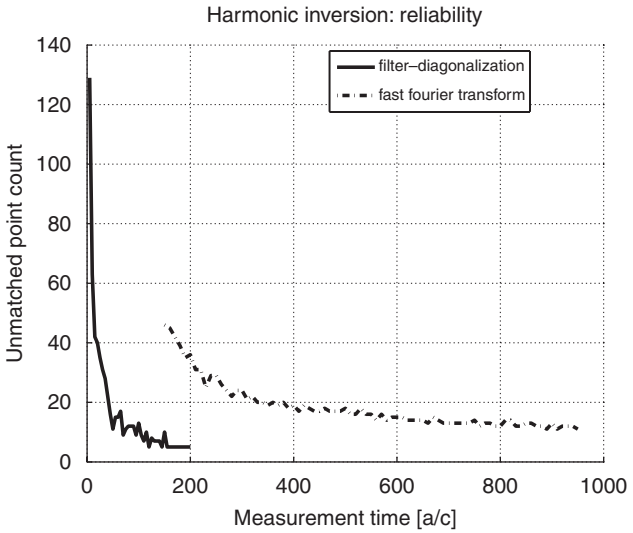

Figure 3. Reliability analysis of frequency diagonalization against measurement time, compared with the Fourier transform. Results shown for the square lattice case.

of the filter-diagonalization algorithm in finding PhC modes as a function of time, and comparing this result against the Fourier transform approach. The results in Figures 2 and 3 show averaged error and missed mode count as a function of measurement time, for both the filter-diagonalization method (implemented using harminv [12]) and the FFT with standard Blackman windowing. The results show that the filter-diagonalization technique dramatically outperforms the FFT, reducing the simulation time needed for our accuracy by a factor of 20.

That the number of unmatched modes converges to five for the filter-diagonalization curve of Figure 3 is an artifact of our comparison algorithm. The remaining five unmatched modes correspond to two uncounted zero frequency points and three degenerate points at band crossovers.

3. RESULTS

To be certain of finding all modes (100% reliability), one could place a sensor at every point of the Yee grid within an IBZ, perform a harmonic inversion at each point, and take the union of the modes found. Since the computational cost of this approach is prohibitive, one rarely does this. Typically one to a few points are selected in a quasirandom fashion, and the results are examined to ensure that they are reasonable. The goal of our investigation is to add some rigor to our understanding of the positional sensitivity of the detectors.

The physics behind the positional dependence is clear. A sensor placed at the node of a mode will have no signal to detect, and will thus miss the mode. We have found that as a detector approaches a node point, the weakness of the signal manifests itself as increased error in the mode location, until eventually the mode is undetected altogether.

DOI: 10.1002/jnm

3.1. Square lattice

In Figures 4 and 5 we have mapped the percentage of found modes as a function of position for TM and TE modes, respectively, for reduced frequencies $0 \leqslant u \leqslant 0.8$. In Figures 6 and 7 the same data are plotted, this time analyzing frequencies $0 \leqslant u \leqslant 1.0$. Each pixel represents the percentage of modes found by a detector/excitation pair placed at the position of the pixel. In all four

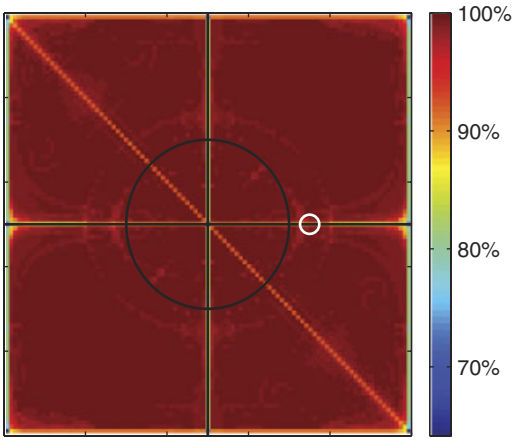

Figure 4. Sensor map of PhC unit cell. Each pixel represents the percentage of TM modes found (in the range $0.0 \leqslant u \leqslant 0.8$) at the position of the pixel. The black contour indicates the dielectric rod boundary. The smaller white circle indicates the location of the band diagram shown in Figure 8.

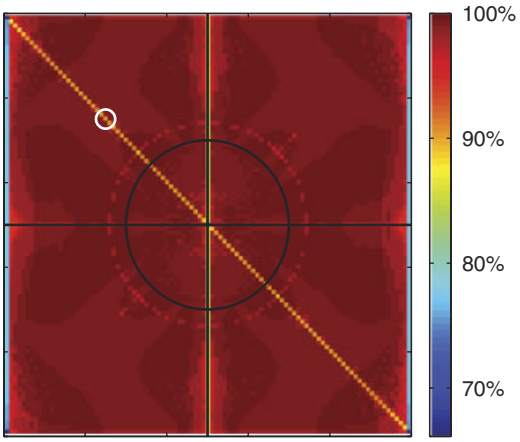

Figure 5. Sensor map of PhC unit cell. Each pixel represents the percentage of TE modes found (in the range $0.0 \leqslant u \leqslant 0.8$) at the position of the pixel. The black contour indicates the dielectric rod boundary. The smaller white circle indicates the location of the band diagram shown in Figure 9.

DOI: 10.1002/jnm

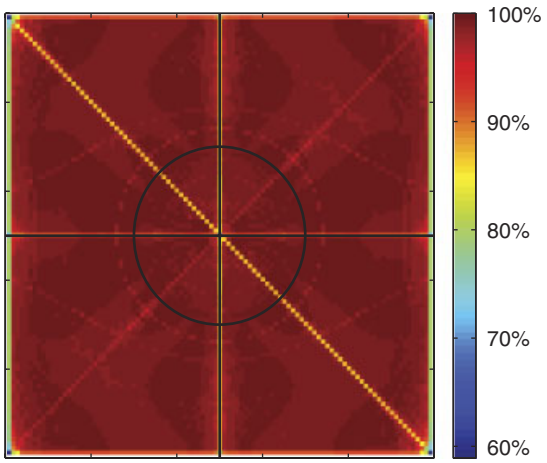

Figure 6. Analogue to Figure 4 with mode frequency range $0.0 \leqslant u \leqslant 1.0$. A distinct hourglass-shaped pattern is visible.

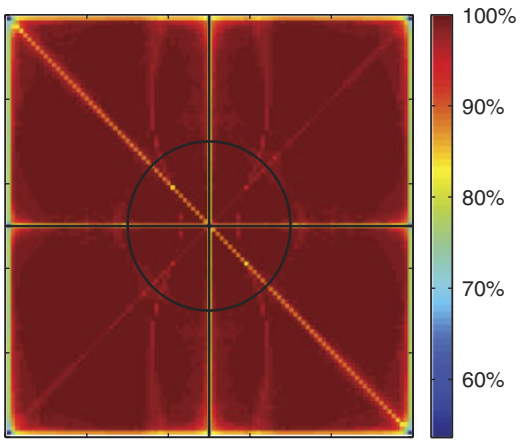

Figure 7. Analogue to Figure 5 with mode frequency range $0.0 \leqslant u \leqslant 1.0$. A faint pattern with the shape of the outline of a horizontally oriented watch wristband is visible.

figures, the map shows a 100×100 pixel matrix, corresponding to 10 000 full band gap diagrams, and 400 000 individual FDTD simulations.

To verify the failure mechanism we have randomly sampled several points with high incidences of missed modes, and analyzed the BDs and field patterns of the missed modes. For all of the sampled modes, we confirmed the existence of a node at the detector position. For the purpose of illustration we present two of these here: one on the horizontal line of symmetry for the TM sensor map, and one on the diagonal line of symmetry for the TE sensor map. The $u = 0.8$ cutoff is marked on the BDs to highlight the location of the high- and low-frequency missed modes.

DOI: 10.1002/jnm

In Figure 8, a string of modes is missing from the 3rd and 6th lowest frequency bands, between the Γ and X points, or the horizontal leg of the IBZ. The inset shows an mode pattern corresponding to one of the missed modes in the string of missing modes of the third lowest frequency band. These missed modes have their nodes coincident with the sensor position, and were therefore undetected. A similar case is shown with a TE mode (Figure 9), but with a node on the diagonal of the IBZ.

At first glance it may be surprising that these maps do not contain all of the symmetries of the system. This is however a natural consequence of the use of Bloch boundary conditions in the FDTD algorithm. Since we enforce the Bloch boundary conditions along a single IBZ, we simulate only the modes propagating along those IBZ vectors, and thus have obtained the node density for the IBZ vectors we have simulated.

These mode count maps contain some notable features. We find that points along the symmetry lines of the system and especially points along the IBZ lines will miss many modes, as all odd modes will have nodes at these locations. Because this effect is stronger along the directions of the IBZ vectors, we see it is best to place detectors in one of the two quadrants orthogonal to the diagonal IBZ vector.

Another observation to be made is that the sensitivity of sensor position is highly localized to the exact location of nodes. One can detect the modes as long as one places the detector at a relatively small distance away from the symmetry points. Aside from the symmetry points, we

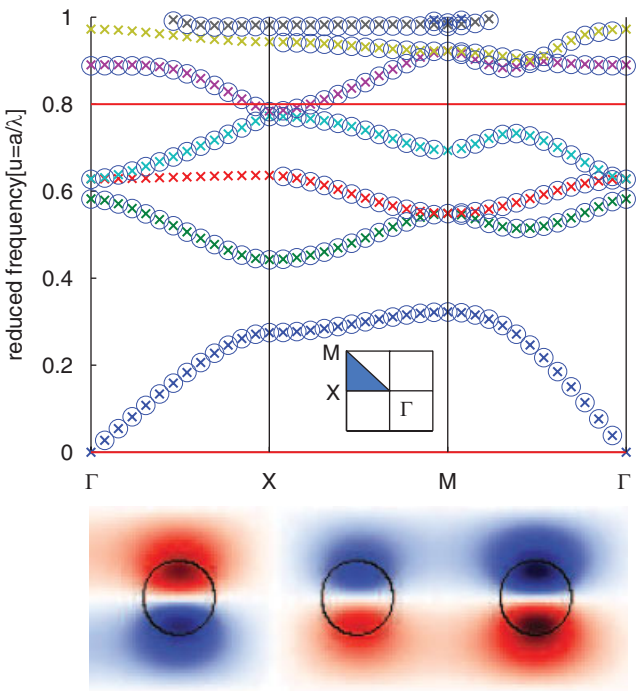

Figure 8. Band diagram for the sensor marked by the white circle in Figure 4. Reference points are marked with an 'X', and test points with 'O's. The line at $u = 0.8$ marks the maximum frequency used for the mode analysis. The inset below shows the mode pattern of an undetected mode. The presence of the node at the sensor position is clearly visible.

DOI: 10.1002/jnm

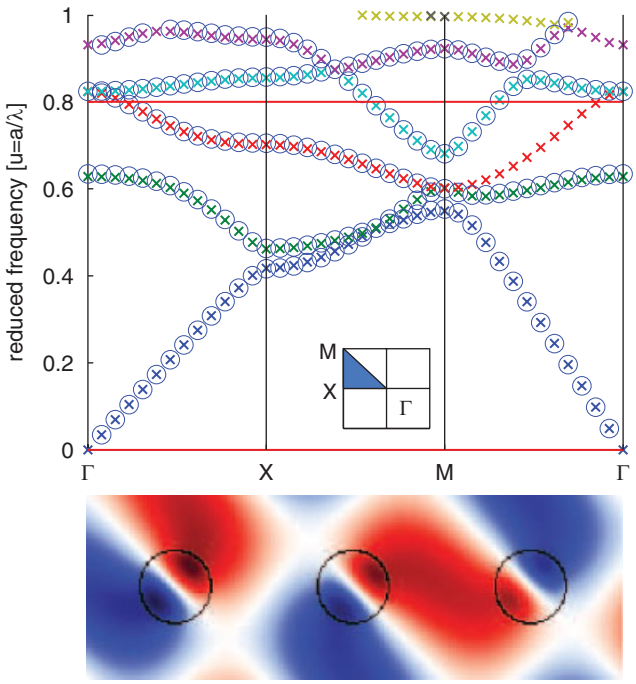

Figure 9. Band diagram for the sensor marked by the white circle in Figure 5. Reference points are marked with an 'X', and test points with 'O's. The line at $u = 0.8$ marks the maximum frequency used for the mode analysis. The inset below shows the mode pattern of an undetected mode. The presence of the node at the sensor position is clearly visible.

find a ring of high nodal density surrounding the dielectric column. These correspond to modes where the bulk of the energy is located within the dielectric. Thus, we find that for lower-order modes of the system (in our system between $0.0 \leqslant u \leqslant 0.8$, a single detector point, located away from symmetry points and away from the material interface, should be sufficient.

For higher-order modes (those above $u = 0.8$), the problem becomes more difficult. For these we find more difficult to comprehend features appearing, specifically the hourglass pattern seen in Figure 6, and the watchband found in Figure 7. For higher-order modes, it is difficult to reduce the problem to a set of simple rules. For these cases, complete results require a few detectors spread out according to the rules layed out above.

3.2. Triangular lattice

Now let us consider the triangular lattice results. Figures 10 and 11 show the percentage of found modes as a function of position for TM and TE modes, respectively, for frequencies $0 \leqslant u \leqslant 0.8$. As in the figures above, each pixel represents the percentage of modes found by a detector/excitation pair placed at the position of the pixel; however, in the triangular lattice figures, maps show a 100×150 pixel matrix.

DOI: 10.1002/jnm

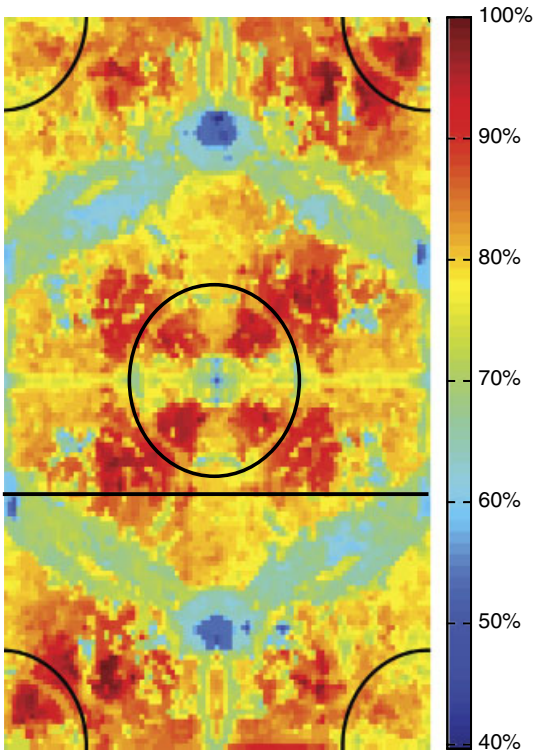

Figure 10. Sensor map of FDTD unit cell for a triangular lattice system, shown the percentage of TM modes found in the range $0.0 \leqslant u \leqslant 0.8$.

Before analyzing the results, we should note that the pixels on the border of the computational domain, i.e. the pixels at the furthest left, right, top, and bottom edges have been truncated from the display, as the filtering algorithm described in Section 2.1.1 cannot be applied at those locations.

We can note several features in these diagrams. As in the square lattice diagrams, there are zones of poor performance along the symmetries of the system. As the square case, the TE map has a region of poor performance around the dielectric. There are, however, two significant differences to the square lattice case: first, the dependence of completion rate on the sensor position is much stronger, and second, the results for the triangular lattice case are much more symmetrical, by which we mean that unlike the square lattice case the positional dependence of the completion rate is not lower for the directions perpendicular to the imposed Bloch vectors.

Both these differences are easily understood in light of the filtering algorithm used to distinguish real modes from folded modes (explained in Section 2.1.1). In order for a mode to be registered as 'found' (and thereby to be considered at all in our benchmarks), the mode must be found both at the selected sensor location, and at its folded location (indeed, it must be found within a certain accuracy and phase shift).

DOI: 10.1002/jnm

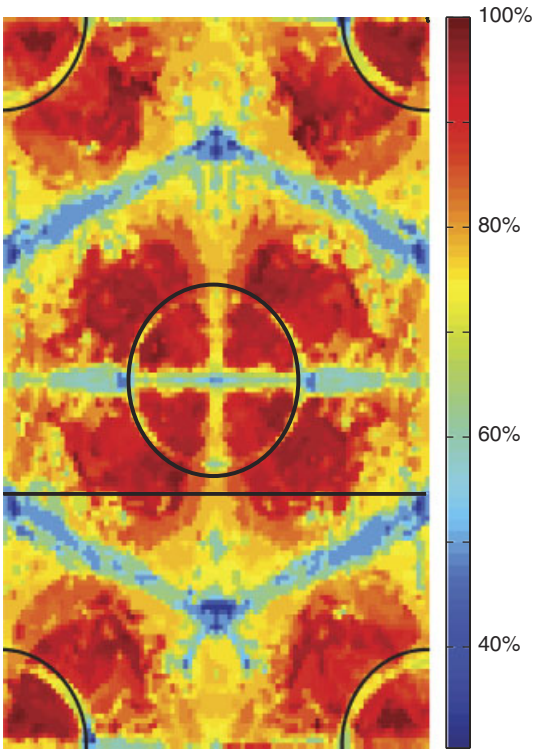

Figure 11. Sensor map of FDTD unit cell for a triangular lattice system, the percentage of TM modes found in the range $0.0 \leqslant u \leqslant 0.8$ is shown.

Consider for a moment what would have been the outcome had we applied the same criteria for the square lattice case. Clearly, a detector placed along the upper right diagonal (the mirror symmetry of the simulated IBZ) would require a detector on the mirrored diagonal. Modes detected (correctly) at this diagonal would not be detected on the phase-shifted detector, as seen in Figure 4. So we see that the algorithm for filtering out folded modes has an unfortunate side effect. By accepting only the intersection of folded IBZs, it magnifies the effect of the positional dependence. The cut-off factors in frequency and phase are additional parameters that must be carefully selected (too coarse and folded modes will be accepted, too fine and modes will be lost). Based on these factors, we believe the modified boundary condition approach should be preferred when possible.

4. CONCLUSIONS

We have developed an algorithm for computing the reliability and accuracy of FDTD simulations of PhCs, and used it to analyze the impact of the density of modal nodes on mode detection. We have mapped the node density of modes for a two canonical PhC device, and shown how they relate to the symmetries of the system. We have found that for lower-order modes a single detector placed away from symmetry points, and away from material discontinuities, is sufficient to detect all modes.

DOI: 10.1002/jnm

We find it more difficult to predict node positions for higher-order modes, implying that more care, and potentially multiple detectors are required when these modes must be detected reliably.

For the triangular lattice system, which necessitates simulating a folded unit cell, we find that the filtering algorithm discussed in Section 2.1.1 amplifies the positional dependence of mode detection, by requiring modes to be detected both at the original detector location and at its folded location. This leads us to believe that the alternative approach (also described in Section 2.1.1) to simulation of non-rectangular lattices, in which the unit cell and boundary conditions are modified, is to be preferred if possible.

In the event that complete mode detection is of critical importance, we can give the following advice based on the above observations: A certain way to detect all modes is to run several simulations, each with a single dipole/sensor pair placed at each grid point on a single IBZ of the unit cell. Taking the union of the modes found will guarantee that no modes have been missed as a result of a node occurring at the measurement point. This approach, however, is computationally expensive. An alternative is to use a random field excitation, as discussed in [5], combined with a dense array (one per voxel) of detectors covering an IBZ of the system being simulated. Care must be taken here to let the simulation ring out sufficiently long for the transient modes to decay.

Finally, although less certain than the above approaches, our results suggest that for most cases it is sufficient to randomly select a few points, away from the material discontinuities and symmetry points of the system, and take the union of the discovered modes. If no new modes are discovered as new dipole/detector points are tested, it is likely the results are complete.

REFERENCES

1. Shih MH, Kuang Q, Mock A, Bagheri M, Hwang EH, O'Brien JD, Dapkus PD. High-quality-factor photonic crystal heterostructure laser. *Applied Physics Letters* 2006; **89**:101104–101106.
2. Nakamura H, Sugimoto Y, Kanamoto K, Ikeda N, Tanaka Y, Nakamura Y, Ohkouchi S, Watanabe Y, Inoue K, Ishikawa H, Asakawa K. Ultra-fast photonic crystal/quantum dot all-optical switch for future photonic networks. *Optics Express* 2004; **12**(26):6606–6614.
3. Johnson SG, Joannopoulos JD. Block-iterative frequency-domain methods for maxwell's equations in a planewave basis. *Optics Express* 2001; **8**(3):173–190.
4. Moreno E, Erni D, Hafner C. Modelling of discontinuities in photonic crystal waveguides with the multiple multipole method. *Physical Review E* 2002; **663**:036618-1–036618-12.
5. Chan CT, Yu QL, Ho KM. Order-n spectral method for electromagnetic waves. *Physical Review B* 1995; **51**(23):16635–16642.
6. Taflove A, Hagness SC, *et al*. *Computational Electrodynamics*: *The Finite-Difference Time-Domain Method* (3rd edn). Artech House: Boston, 2005.
7. Joannopoulos JD, Meade R, Winn J. *Photonic Crystals*, *Molding the Flow of Light*. Princeton University Press: Reading, MA, 1995.
8. Farjadpour A, *et al*. Improving accuracy by subpixel smoothing in the finite-difference time domain. *Optics Letters* 2006; **31**:2872–2974.
9. Main J. Use of harmonic inversion techniques in semiclassical quantization and analysis of quantum spectra. arXiv:chao-dyn/9902008v1.
10. Wall MR, Neuhauser D. Extraction, through filter diagonalization, of general quantum eigenvalues or classical normal mode frequencies from a small number of residues of a short-time segment of a signal. *Journal of Chemical Physics* 1995; **102**:8011–8022.
11. Burr GW, Farjadpour A. Balancing accuracy against computation time: 3-d FDTD for nanophotonics device computation. *Proceedings of the SPIE* 2005, **5733**: 336–347.
12. Johnson SG. *harminv*, http://ab-initio.mit.edu/wiki/index.php/Harminv.

DOI: 10.1002/jnm

AUTHORS' BIOGRAPHIES

Glen Stark earned a BSc in Physics from the Georgia Institute of Technology. He received a scholarship from the World Student Fund to visit the ETH Zürich as a guest scholar, during which he studied mathematical physics. Thereafter he took a masters degree in Computational Physics from ETH Zurich. Since 2003 he has been working on his PhD on FDTD techniques for photonics in the Communication Photonics Group (Electronics Lab, ETH Zurich).

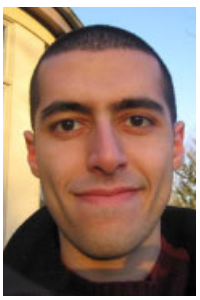

Matthew Mishrikey graduated with BS (2002), and MEng (2005) degrees in electrical engineering and computer science from the Massachusetts Institute of Technology. His graduate coursework was in control theory, electromagnetics, and electrohydrodynamics. For his master's degree, he developed a system for the detection and mitigation of electrical arcing in automotive wiring harnesses. He worked as a research engineer at the BMW Group headquarters in Munich, Germany, where he worked on recuperative energy systems and prototype vehicles with electrical starter-generators. Matthew is currently a doctoral student at the Laboratory for Electromagnetic Fields and Microwave Electronics. His current research is in the field of metamaterials for microwave shielding as well as for optical applications. His work focuses on numerical techniques for analysing, designing, and optimizing photonic structures. He helps teach basic courses in antenna theory and fundamental electromagnetics. Matthew is originally from Philadelphia, PA, U.S.A., and has been living in Zurich, Switzerland since 2005.

Franck Robin received the engineering degree in material sciences and semiconductor physics and the Master's degree in integrated electronics from the National Institute for Applied Sciences (INSA), Lyon, France, in 1996 and 1999, respectively, and the PhD degree from the Swiss Federal Institute of Technology (ETH), Zurich, Switzerland, in 2002. He has been active in the fields of InP-based technology applied to high-frequency electronics and integrated optics for over 10 years. He was group leader of the Communication Photonics Group of the ETH Zurich. Dr F. Robin has authored or co-authored ca. 130 papers in peer-reviewed journals and conference proceedings. He is now managing the research projects of an innovative Swiss medical device company.

Heinz Jäckel has been full Professor at the Electronics Laboratory of the Swiss Federal Institute of Technology, ETH Zurich since 1993 heading the 'High Speed Electronics and Photonics' group (http://www.ife.ee.ethz.ch/, http://www.photonics.ee.ethz.ch/). Prof. Jckel completed his PhD in EE at the ETH Zurich in 1979. In 1980 he joined the IBM Research Division where he held scientific and management positions for 13 years in IBM Rüschlikon, Switzerland, and IBM Yorktown Heights, U.S.A. During this time he carried out research in superconducting Josephson Junction Computers, GaAs-Mesfet ICs and Optoelectronics. In electronics the research activities of his group concentrate on: (1) development of III/V-technology, (2) design and characterization of ultrafast InP-HBT transistors for +100 Gb/s

DOI: 10.1002/jnm

electronics and (3) multi-10 GHz RF and digital 10-40 Gb/s CMOS IC design. In the area of ultra-dense and Tb/s lightwave communication research topics are: (1) integrated InP-based mode-locked diode lasers, (2) all-optical switches for all optical signal processing at Tb/s data rates and (3) planar InP-based photonic crystals. Heinz Jckel has authored or co-authored over a 100 publications, in addition he holds some 20 patents.

Christian Hafner received his diploma, his PhD degree, and venia legendi from the ETH Zurich, in 1975, 1980, and 1987, respectively. Since 1999 he is Professor at the ETH and head of the Computational Optics Group at the Laboratory for Electromagnetic Fields and Microwave Electronics. He is a member of the Electromagnetics Academy. Christian Hafner developed the Generalized Multipole Technique (a semi-analytical method for computational electromagnetics) and various Maxwell solvers, namely the Multiple Multipole Program (MMP)-that was awarded in 1990 the second prize of the Seymour Cray award for scientific computing-finite difference solvers in time and frequency domain, mode matching techniques, parameter estimation techniques, and the MaX-1 software package for computational electromagnetics and optics. He also developed various numerical optimizers based on evolutionary strategies, genetic algorithms, genetic program ming, and many more. His current research focus is on plasmonics, metallo-dielectric photonic crystals, optical antennas, nearfield optical microscopy, plasmonic sensors, ultra-dense-integrated optics, composite-doped metamaterials including materials operating at microwaves and low frequencies.

Rudiger Vahldieck received the Dipl-Ing and Dr-Ing degrees in electrical engineering from the University of Bremen, Bremen, Germany, in 1980 and 1983, respectively. From 1984 to 1986, he was a Postdoctoral Fellow with the University of Ottawa, Ottawa, Ont., Canada. In 1986, he joined the Department of Electrical and Computer Engineering, University of Victoria, Victoria, BC, Canada, where he became a Full Professor in 1991. During Fall and Spring 1992-1993, he was a Visiting Scientist with the Ferdinand-Braun-Institut für H—chstfrequenztechnik, Berlin, Germany. In 1997, he became a Professor for electromagnetic field theory with the Swiss Federal Institute of Technology, Zurich, Switzerland, and became Head of the Laboratory for Electromagnetic Fields and Microwave Electronics (IFH) in 2003. Since 1981, he has authored or coauthored over 230 technical papers in books, journals, and conferences, mainly in the field of microwave computer-aided design (CAD). His research interests include computational electromagnetics in the general area of electromagnetic compatibility (EMC), particularly for computer-aided design of microwave, millimeter-wave, and opto-electronic-integrated circuits. Prof. Vahldieck is a member of the Editorial Board for the IEEE Transaction on Microwave Theory and Techniques. From 2000 to 2003, he was an associate editor for the IEEE Microwave and Wireless Components Letters and has been its editor-in-chief since 2004. Since 1992, he has served on the Technical Program Committee (TPC) of the IEEE Microwave Theory and Techniques Society (IEEE MTT-S) International Microwave Symposium (IMS), the IEEE MTT-S Technical Committee on Microwave Field Theory, and in 1999, on the TPC of the European Microwave Conference. From 1998 to 2003 he was chapter chairman of the IEEE Swiss Joint Chapter on Microwave Theory and Techniques (MTT), Antennas and Propagation (AP), and electromagnetic compatibility (EMC). He was the recipient of the J. K. Mitra Award presented by the Institute of Electronics and Telecommunication Engineers (IETE) (1996) for the best research paper in 1995. He was corecipient of the outstanding publication award of the Institution of Electronic and Radio Engineers in 1983. He is the past president of the 2000 International Zurich Seminar on Broadband Communications (IZS'2000), president, and general chairman of the International Zurich Symposium on Electromagnetic Compatibility (EMC Zurich).

DOI: 10.1002/jnm

Daniel Erni received a diploma degree from the Applied University in Rapperswil (HSR) in 1986, and a diploma degree from ETH Zürich in 1990, both in electrical engineering. Since 1990 he has been working at the Laboratory for Electromagnetic Fields and Microwave Electronics, ETH Zurich, where he got his PhD degree in 1996. From 1995 to 2006 he has been the founder and head of the Communication Photonics Group at ETH Zurich. Since October 2006 he is a full professor for General and Theoretical Electrical Engineering at the University of Duisburg-Essen, Germany (http://www.ate.uni-due.de/). His current research includes laser physics, advanced data transmission schemes (i.e. O-MIMO) in board-level optical interconnects, optical on-chip interconnects, ultra-dense integrated optics, nanophotonics, plasmonics, electromagnetic and optical metamaterials and quantum optics. On the system level, Daniel Erni has pioneered the introduction of numerical structural optimization into dense integrated optics device design. He has authored and co-authored over 300 publications and is a Fellow of the Electromagnetics Academy, as well as a member of the Swiss Physical Society (SPS), of the German Physical Society (DPG), of the Optical Society of America (OSA), and of the IEEE.

DOI: 10.1002/jnm